Journal of Antimicrobial Chemotherapy
doi:10.1093/jac/dkl182

JAC

Antifungal and antimycobacterial activity of new imidazole and triazole derivatives. A combined experimental and computational approach

Elena Banfi[1]*, Giuditta Scialino[1], Daniele Zampieri[2], Maria Grazia Mamolo[2], Luciano Vio[2], Marco Ferrone[3], Maurizio Fermeglia[3], Maria Silvia Paneni[3] and Sabrina Pricl[3]

[1]Microbiology Laboratory, Department of Biomedical Sciences, University of Trieste, I-34127 Trieste, Italy; [2]Department of Pharmaceutical Sciences, University of Trieste, I-34127 Trieste, Italy; [3]Molecular Simulation Engineering (MOSE) Laboratory, Department of Chemical Engineering, University of Trieste, I-34127 Trieste, Italy

Received 23 January 2006; returned 22 February 2006; revised 12 April 2006; accepted 18 April 2006

***Objectives*: To synthesize new antimycobacterial and antifungal drugs that act by binding to sterol 14α-demethylase (14DM) and to characterize the drug–target protein interactions using computer-based molecular simulations.**

***Methods*: Different series of imidazole and triazole derivatives having an azomethine linkage to pyridine 2-carboxamidrazone were designed and synthesized. Molecular dynamic simulations of the sterol 14DM (a mixed-function oxidase involved in sterol synthesis in eukaryotic and prokaryotic organisms) complexed with new azole derivatives have been performed to both qualify and quantify the protein–ligand interactions. MICs of the compounds were evaluated by reference assay and by recently developed Microdilution Resazurin Assay (MRA).**

***Results*: Halogenated derivatives showed good activity, with an MIC_{90} of 1 mg/L against 33 Candida spp. clinical strains; most compounds also had inhibitory activity against *Mycobacterium tuberculosis* reference and clinical strains, with MICs in the range 4–64 mg/L. Molecular modelling investigations showed that the active new compounds may interact at the active site of both the fungal and the mycobacterial cytochrome P450-dependent sterol-14α-demethylase and that the calculated binding free energy values are in agreement with the corresponding MIC values.**

***Conclusions*: The combined experimental and computational approach can be helpful in targeted drug design, thus yielding valuable information for the synthesis and prediction of activity of a second generation of inhibitors.**

Keywords:

Introduction

Tuberculosis is a significant public health problem in both industrialized and developing countries and is responsible for more than two million deaths each year. Therapy is complicated due both to the requirement for prolonged treatment with a combination of drugs and the emergence of drug-resistant strains. In addition, severe opportunistic fungal infections, particularly caused by *Candida* spp., are increasing in incidence, particularly in immunocompromised patients. There is a continuing need for new and effective drugs active against both *Mycobacterium tuberculosis* and fungi. To this end, we designed a series of compounds in which the aryl-azolyl-ethane moiety, present in many azole antifungal drugs, is linked through an azomethine linkage to pyridine-2-carboxamidrazone, a chemical moiety that has been shown to possess an important mycobacterium killing activity.[1,2] Many azole derivatives targeting sterol demethylase have also been shown to possess interesting antimycobacterial activity associated with good antifungal activity.[3–5] Sterol 14α-demethylase (14DM) is a mixed-function oxidase involved in sterol synthesis in eukaryotic organisms; moreover, the completion of the *M. tuberculosis* genome project revealed

*Corresponding author. Tel: +39-40-5587187; Fax: +39-40-351668; E-mail: banfi@dsb.units.it

that a protein having homology to mammalian 14DMs might be present in this bacterium.[6]

In this study we synthesized new imidazolyl and triazolyl-pyridinecarboxamidrazone derivatives and measured their antibacterial, antifungal and antitubercular activities *in vitro* by standard and newly developed microdilution assays.[7] Furthermore, in this paper we propose a combined approach for evaluating these new drugs, based on experimental evidence and on computer-aided molecular modelling. Models in science are employed to simplify, analysing single phenomena believed to be critical. Models give also a didactical combined representation of structure and molecular properties of different molecules. Mathematical modelling techniques give also a simulation of a chemical reaction step.[8] We have already employed mathematical modelling techniques for the computation of physical states of newly synthesized molecules, and applied it to quantify their interactions with the target fungal enzyme cytochrome P450-dependent sterol 14α-demethylase CYP51 in the ergosterol biosynthesis pathway.[9] In the present work we propose the prediction of the interaction of new imidazole and triazole derivatives of 2-pyridinecarboxamidrazone with the target *M. tuberculosis* and *Candida albicans* enzymes cytochrome P450-dependent 14DM through a computer modelling of drug–enzyme complexes. Relative free energies of association of the molecules have been calculated and related to the obtained experimental data.

Materials and methods

Strains and media

Reference strain *Staphylococcus aureus* ATCC 20202 was employed to evaluate the antibacterial activity of the new molecules. A total of 21 strains of *C. albicans* and 12 strains of *Candida glabrata*, all clinical isolates, were selected to test the antifungal activity. *M. tuberculosis* reference strain H37Rv and two respiratory isolates of *M. tuberculosis*, identified by classical culture and biochemical methods and by DNA probe (GeneProbe, San Diego, CA, USA), were employed to measure the antitubercular activity of the new molecules. The drug susceptibility of *Mycobacterium* clinical isolates was measured by the agar proportion test and by BACTEC MGIT manual system. Bacteria were grown in LB medium to a density of 0.5–1 $\times$ 10^4 cfu/mL; *Candida* strains were grown on Sabouraud agar plates (Difco) and resuspended in RPMI medium (Sigma) to a density of 0.5–1 $\times$ 10^4 cfu/mL. *Mycobacterium* strains were maintained on Lowenstein–Jensen medium (Becton Dickinson) and grown 14 days in Middlebrook 7H9 broth supplemented with 10% OADC (Becton Dickinson), 0.2% glycerol and 0.1% Bacto Casitone (Difco) to a bacterial density of 0.5–1 $\times$ 10^4 cfu/mL.

Chemicals

Twelve new N^1-[1-aryl-2-(1*H*-imidazol-1-yl and 1*H*-1,2,4-triazol-1-yl)-ethylidene]-pyridine-2-carboxamidrazone derivatives, **2 a–l**, have been synthesized and their physical data measured according to the procedure reported in the paper by Mamolo *et al.*[9] Stock solutions of each chemical were prepared in DMSO at a concentration of 4 mg/mL and stored until used in biological assays. Reference antibiotics were also employed for comparison.

Antimicrobial susceptibility testing

The *in vitro* antifungal activity of derivatives **2 a–l** has been tested against *Candida* spp. clinical isolates, measuring MICs by a microdilution RPMI reference method.[10] Miconazole and amphotericin B were used as reference test compounds. Each MIC was determined twice in duplicate experiments after 24 and 48 h incubation time against 33 C*andida* spp. strains. The antibacterial activity was evaluated by a standard broth-dilution method. The *in vitro* antitubercular activity of derivatives **2 a-l** has been evaluated measuring MICs by MRA—a new Microdilution Resazurin Assay—in liquid medium and within 8 days of incubation, as previously described.[7] Isoniazid and rifampicin were used as positive controls in this case. Briefly, twofold dilutions of each compound were prepared from stock solutions in 96-well plates in complete 7H9 broth, final compound concentrations being 128–0.125 mg/L. An aliquot of 20 μL of each bacterial suspension was added to 180 μL of drug-containing culture medium. The plates were sealed and incubated 7 days at 37°C. Five microlitres of resazurin (Sigma Aldrich, 10 mg/mL sterile water stock solution) were added per well, and the plates were allowed to incubate at 37°C for additional 24 h. Plates were finally read by visual inspection for colour change from blue to pink in wells containing live mycobacteria. MIC was defined as the lowest drug concentration that prevented resazurin colour change.[7] MICs were determined twice in duplicate experiments and were considered bactericidal by viable counts from blue wells when 99% cfu were inhibited. DMSO was also evaluated and was always devoid of inhibiting activity up to the concentration of 2% (v/v).

Computational methods

The starting structure of the cytochrome P450 sterol 14DM of *M. tuberculosis* was taken from the Protein Data Bank (PDB entry: 1E9X).[11] Geometry refinement was carried out using the *Sander* module of AMBER 7[12] via a combined steepest descent-conjugate gradient algorithm. The *parm94* version[13] of the all-atom AMBER force field was applied for protein relaxation, with the haem model parameters of Paulsen and Ornstein.[14] The GB/SA continuum solvation model[15] was used to mimic a water environment.

The 3D model structure of the same enzyme from *C. albicans*, presently not available in the PDB, was built by a combination of homology-based techniques.[16] Briefly, we first used the *Biopolymer* and *Binding Site* modules of the INSIGHTII software (v.2001, Accelrys Inc., San Diego, CA, USA) to generate a sequence alignment between the *C. albicans* and *Candida tropicalis*, *C. glabrata*, *Candida krusei* and *M. tuberculosis* P450s (Swiss-Prot accession numbers P10613, P14263, P50859, Q02315 and P0A512, respectively). The result of the multiple alignments is reported in Figure 1. Subsequently, the MODELLER program[17,18] was employed to build a preliminary 3D model of the 14DM of *C. albicans* based on the alignment obtained in the previous step and the 3D crystal structure of the *M. tuberculosis*[11] enzyme as reference protein. The original 3D model proposed by Boscott and Grant,[19] and subsequently used by Kelly *et al.*,[20] was also used as a putative 3D structure in this phase. According to the method followed, the structurally conserved regions (SCRs) of the modelled protein were first identified and modelled, assigning the spatial coordinates directly from those of the reference proteins. The coordinates for the variable regions (the connections between these pre-built pieces), such as loops, were calculated either using the loop search procedure[21–23] or, when these regions were confined to a few amino acids, using the replacement method.[24] The complete 3D model structure of the *C. albicans* sterol 14DM obtained was refined

```
albicans        MAIV---------ETVIDGINYFLSLSVTQQISILLGVPFVYNLVWQYLYSLRKDRAPLV 51
glabrata        MSTENTSLVVELLEYVKLGLSYFQALPLAQRVSIMVALPFVYTITWQLLYSLRKDRPPLV 60
tropicalis      MAIV---------DTAIDGINYFLSLSLTQQITILVVFPFIYNIAWQLLYSLRKDRVPMV 51
krusei          M------------------------------------------------------------ 1
tuberculosis    MSAV---------------------------------------------------------- 4
                *

albicans        FYWIPW-----------FGSAASYGQQPYEFFESCRQKYGDVFSFMLLGKIMTVYLGPKG 100
glabrata        FYWIPW-----------VGSAIPYGTKPYEFFEDCQKKYGDIFSFMLLGRIMTVYLGPKG 109
tropicalis      FYWIPW-----------FGSAASYGMQPYEFFEKCRLKYGDVFSFMLLGKVMTVYLGPKG 100
krusei          ----PW-----------VGSAVVYGMQPYEFFENCRKQHGDVFSFLLLGKVMTVYLGPKG 46
tuberculosis    ------ALPRVSGGHDEHGHLEEFRTDPIGLMQRVRDECGDVGTFQLAGKQVVLLSGSHA 58
                      *    :   *  ::: : : **: :* * *: : :  * :

albicans        HEFVFNAKLSDVSAEDAYKHLTTPVFGKGVIYDCPNSRLMEQKKFAKFALTTDSFKRYVP 160
glabrata        HEFIFNAKLADVSAEAAYSHLTTPVFGKGVIYDCPNHRLMEQKKFVKGALTKEAFVRYVP 169
tropicalis      HEFIYNAKLSDVSAEEAYTHLTTPVFGKGVIYDCPNSRLMEQKKFAKFALTTDSFKTYVP 160
krusei          HEFVLNAKLSDVSAEDAYTHLTTPVFGKGVIYDCPNWKLMEQKKFAKVALTKESFIRYVP 106
tuberculosis    NEFFFRAGDDDLDQAKAYPFM-TPIFGEGVVFDASPERRKEM--LHNAALRGEQMKGHAA 115
                :**   *   *:    **  : **:**:**::*    :  *   : : **  : :  :

albicans        KIREEILNYFVTDESFKLKEKTHGVANVMKTQPEITIFTASRSLFGDEMRRIFDRSFAQL 220
glabrata        LIAEEIYKYFRNSKNFKINENNSGIVDVMVSQPEMTIFTASRSLLGKEMRDKLDTDFAYL 229
tropicalis      KIREEVLNYFVNDVSFKTKERDHGVASVMKTQPEITIFTASRCLFGDEMRKSFDRSFAQL 220
krusei          LIKDEMLKYFNAN--F---RGDSGKTDVLKSQSEMTLFTASRSLFGDALRNRLDASYAEM 161
tuberculosis    TIEDQVRRMIAD-------WGEAGEIDLLDFFAELTIYTSSACLIGKKFRDQLDGRFAKL 168
                 * :::   :             *   ::    *:*::*:*  *:*  :*  :*  :* :

albicans        YSDLDKGFTPINFVFPNLPLPHYWRRDAAQKKISATYMKEIKSRRERGDID-PNRDLIDS 279
glabrata        YSDLDKGFTPINFVFPNLPLEHYRKRDHAQQAISGTYMSLIKERREKNDIQ--NRDLIDE 287
tropicalis      YADLDKGFTPINFVFPNLPLPHYWRRDAAQRKISAHYMKEIKRRRESGDID-PKRDLIDS 279
krusei          YSDLDKGFTPLNFVFSYLPLPNYWKRDAAHKNISNTYLDLINTKRAGGEIK--NEDLVDA 219
tuberculosis    YHELERGTDPLAYVDPYLPIESFRRRDEARNGLVALVADIMNGRIANPPTDKSDRDMLDV 228
                * :*::*  *: :*   **:  : :** *:  :       :: :           *::*

albicans        LLIHSTYKDGVKMTDQEIANLLIGILMGGQHTSASTSAWFLLHLGEKPHLQDVIYQEVVE 339
glabrata        LMKNSTYKDGTKMTDQEIANLLIGVLMGGQHTSAATSAWCLLHLAERPDVQEELYQEQMR 347
tropicalis      LLVNSTYKDGVKMTDQEIANLLIGVLMGGQHTSASTSAWFLLHLAEQPQLQDDLYEELTN 339
krusei          LLKNSVYKDGTRMTDEELAHLMIGVLMGGQHTSSATSAWFLLHLGEKPQLQEEIYREIQS 279
tuberculosis    LIAVKAETGTPRFSADEITGMFISMMFAGHHTSSGTASWTLIELMRHRDA----YAAVID 284
                *:         ::: :*:: ::* ::: *:***: *::* *: *  :       *

albicans        LLKEKGGDLNDLTYEDLQKLPSVNNTIKETLRMHMPLHSIFRKVTNPLRIPETNYIVPKG 399
glabrata        VLN---NDTKELTYDDLQNMPLLNQMIKETLRLHHPLHSLFRKVMRDVAIPNTSYVVPRD 404
tropicalis      LLKEKGGDLNDLTYEDLQKLPLVNNTIKETLRMHMPLHSIFRKVMNPLRVPNTKYVIPKG 399
krusei          VLGEN--FERELTYDDLQKLDLVNATIKETLRLHMPLHSIFRKVTRDLPVPNTSYIVPKG 337
tuberculosis    ELDELYGDGRSVSFHALRQIPQLENVLKETLRLHPPLIILMRVAKGEFEVQ--GHRIHEG 342
                 *         :::  *:::  ::  :*****:* **  ::*       :    : :

albicans        HYVLVSPGYAHTSERYFDNPEDFDPTRWDTAAAKANSVSF-----NSSDEVDYGFGKVSK 454
glabrata        YHVLVSPGYTHLQEEFFPKPNEFNIHRWDGDAASSSAA--------GGDEVDYGFGAISK 456
tropicalis      HYVLVSAGYAHTSDRWFEHPEHFNPRRWESDDTKASAVSF-----NSEDTVDYGFGKISK 454
krusei          HYVLISPGYTMLSERYFPNASEFQPHRWDEIKSIDGGISFGAEGENAKETVDYGFGKISK 397
tuberculosis    DLVAASPAISNRIPEDFPDPHDFVPARYEQPRQE-------------------------- 376
                  *  *   :      *     *   *::

albicans        GVS-----SPYLPFGGGRHRCIGEQFAYVQLGTILTTFVYNLRWTI--DGYKVP---DPD 504
glabrata        GVS-----SPYLPFGGGRHRCIGELFAYCQLGVLMSIFIRTMKWRYPTEGETVP---PSD 508
tropicalis      GVS-----SPYLPFGGGRHRCIGEQFAYVQLGTILTTYIYNFKWRL--NGDKVP---DVD 504
krusei          GVA-----SPYLPFGGGRHRCT------------------------------------- 414
tuberculosis    ---DLLNRWTWIPFGAGRHRCVGAAFAIMQIKAIFSVLLREYEFEMAQ----PPESYRND 429
                         ::*** *****

albicans        YSSMVVLPTEPAEIIWEKRET-CMF 528
glabrata        FTSMVTLPTAPAKIYWEKRHPEQKY 533
tropicalis      YQSMVTLPLEPAEIVWEKRDT-CMV 528
krusei          -------------------------
tuberculosis    HSKMVVQLAQPACVRYRRRT---GV 451
```

Figure 1. Alignment of the amino acid sequences of cytochrome P450 sterol 14-α demethylase of *C. albicans*, *C. tropicalis*, *C. glabrata*, *C. krusei* and *M. tuberculosis*. The secondary structural motifs are highlighted in bold and coloured according to the following schema: red: helices; blue: sheets, green: the N-terminal membrane-spanning domain (residues 3–43). Amino acids conserved in all five sequences are indicated by the symbol *, while conservative mutations are indicated by the symbol.

using several energy minimization rounds. The side chain positions were first optimized, keeping the protein backbone fixed. This constraint was then removed, and further protein relaxation was performed until the conjugate gradient algorithm converged.

At this point, all ionizable residues were switched on to their standard ionization state at neutral pH in both *M. tuberculosis* and *C. albicans* 14DM models and, to achieve electroneutrality, a suitable number of counterions were added, in the positions of largest

electrostatic potential, as determined by the module *Cion* within AMBER 7. The two proteins were then subjected to energy minimization: steepest descents were carried out. After energy minimization, 500 ps molecular dynamics (MD) simulations were performed, at constant temperature[25] (T = 25°C) and pressure[26] (P = 1 atm) in the GB/SA water environment,[15] using an integration time step[27] of 1 fs, and the applications of the Shake algorithm.[28] Conformers of each protein were collected every 2 ps, the energy profiles were analysed and, among the 250 saved conformers, 40 conformers for each system showing the lowest total energies were selected and their 3D structures were superimposed. Their root mean square deviation (rmsd) values were 0.90 and 1.2 Å for *M. tuberculosis* and *C. albicans*, respectively. Of these, the conformer with the lowest energy for each system was chosen for drug binding energy calculations. The quality of the *C. albicans* sterol 14DM model was further assessed by using the well-validated programs PROCHECK[29] and WHATIF.[30] The final statistical analysis of the Ramachandran plot showed that 97% of the main-chain dihedral angles were found in the most favourable region, thus confirming the good quality of the 3D model of our *C. albicans* P540 enzyme.

The model structures of all azole compounds were generated using the *Biopolymer* module of INSIGHTII. All molecules were subjected to an initial energy minimization. A conformational search was carried out using a well-validated combined molecular mechanics/molecular dynamics simulated annealing (MM/MDSA) protocol,[31–34] and only the structures corresponding to the minimum energy were used for further modelling. The electrostatic charges for the geometrically optimized drug molecules were obtained by restrained electrostatic potential fitting.[35–37]

The optimized structures of the active compounds were docked into both enzyme active sites following a validated procedure,[32–34] which employs the software AUTODOCK 3.0.[38] In the generation of the electrostatic grid maps, the distance-dependent relative permittivity of Mehler and Solmajer[39] was applied. For the docking of each compound to the protein, 300 Monte Carlo/Simulated Annealing (MC/SA) runs were performed. Following the docking procedure, all structures of azole compounds were subjected to cluster analysis with a tolerance of 1 Å for an all-atom rms deviation from a lower-energy structure representing each cluster family. In the absence of any relevant crystallographic information for this series of compounds, the structure of each resulting complex characterized by the lowest interaction energy was selected for further evaluation. Each best drug–protein complex resulting from the automated docking procedure was further refined in the AMBER suite using the quenched molecular dynamics method (QMD).[40–42]

For the calculation of the binding free energy in water, the best energy configuration of each complex resulting from the previous step was solvated by a cubic box of TIP3P water molecules[43] extended at least 10 Å in each direction from the solute. The periodic boundary conditions with constant pressure[26] of 1 atm were applied, and long-range non-bonded van der Waals interactions were truncated by using an 8 Å residue-based cut-off. The particle mesh Ewald method[44] was used to treat the long-range electrostatics. Unfavourable interactions within the structures were relieved with steepest descent followed by conjugate gradient energy minimization. Each system was gradually heated to 25°C in three intervals, equilibrated for 25 ps at 25°C and finally subjected to 400 ps of data collection runs. A total of 400 snapshots were saved during data collection period, one snapshot per 1 ps of MD simulation.

The binding free energy ΔG_{bind} of each drug–14DM complex in water was calculated according to the so-called Molecular Mechanics/Poisson–Boltzmann Surface Area (MM/PBSA) procedure proposed by Srinivasan *et al.*,[45] which will be briefly described below. According to this method, ΔG_{bind} is calculated as,

$$\Delta G_{bind} = \Delta E_{MM} + \Delta G_{solv} - T\Delta S \quad (1)$$

where

$$\Delta G_{solv} = \Delta G_{PB} + \Delta G_{NP} \quad (2)$$

ΔE_{MM} denotes the sum of molecular mechanics (MM) energies of the molecules and can be further split into contributions from electrostatic (E_{EL}) and van der Waals (E_{vdW}) energies:

$$\Delta E_{MM} = \Delta E_{EL} + \Delta E_{vdW} \quad (3)$$

The terms in Equation (3) were calculated by using the *Carnal* and *Anal* modules of AMBER 7. The polar component of ΔG_{solv} [i.e. ΔG_{PB} in Equation (2)] was evaluated with the Poisson–Boltzmann (PB) approach.[46] All atomic charges were taken from the Cornell *et al.*[13] force field and from our *ab initio* calculations (see above), since these are consistent with the MM energy calculations. However, as suggested by Chong *et al.*,[47] the atomic radii were taken from the parse parameter set instead of the *parm94* force field set because of the small size of hydrogens in the latter. The numerical solution of the linearized PB equations was solved on a cubic lattice by using the iterative finite-difference method implemented in the DelPhi software package.[48] The non-polar contribution to the solvation energy [i.e. ΔG_{NP} in Equation (2)] was calculated as $\Delta G_{NP} = \gamma$ (SASA) + β, in which γ = 0.00542 kcal/Å^2, β = 0.92 kcal/mol and SASA is the solvent-accessible surface estimated with the MSMS program.[49]

The normal-mode analysis approach[50,51] was followed to estimate the last parameter, i.e. the change in solute entropy upon association $-T\Delta S$.

Results

We designed and synthesized a series of 12 compounds in which the 1-aryl-2-(1H-azol-1-yl)-ethane moiety, characteristic of many azole antifungal drugs, is connected via an azomethine linkage to pyridine-2-carboxamidrazone. Figure 2 reports the scheme of the synthesis of these 12 new N^1-[1-aryl-2-(1*H*-imidazol-1-yl and 1 *H*-1,2,4-triazol-1-yl)-ethylidene]-pyridine-2-carboxamidrazone derivatives, leading to compounds **2a–l**. Evaluation of the antibacterial activity of our new compounds showed a slight inhibitory effect on Gram-positive reference strain *S. aureus* by aryl-imidazolyl derivatives, with an MIC in the range 16–32 mg/L, while no inhibitory effect was shown by triazolyl pyridine-carboxamidrazone compounds (MIC > 128 mg/L). Some of the new compounds had a remarkable antifungal activity, comparable with that of amphotericin B and of miconazole, as reported in Table 1. Derivatives **2 a–e** had an MIC_{90} in the range 0.125–2 mg/L after 24 h and 0.5–4 mg/L after 48 h incubation time against 21 *C. albicans* clinical strains. Derivatives **2 a–e** had an MIC_{90} in the range 0.5–8 mg/L after 24 h and 1–16 mg/L after 48 h incubation time against 12 *C. glabrata* clinical strains. In this case, the most active compounds were found to be the halogenated (Br and Cl) derivatives **2b** and **2c**, with MIC_{90} of 1 mg/L against *Candida* spp. Compounds **2 f–j** had MIC_{90} of 64 mg/L for *Candida* spp; on the other hand, compounds **2 k** and **l** showed an MIC_{90} of 8 mg/L against *C. albicans* and an MIC_{90} of 16 mg/L against *C. glabrata*. We already performed a preliminary study in order to verify whether and how the newly

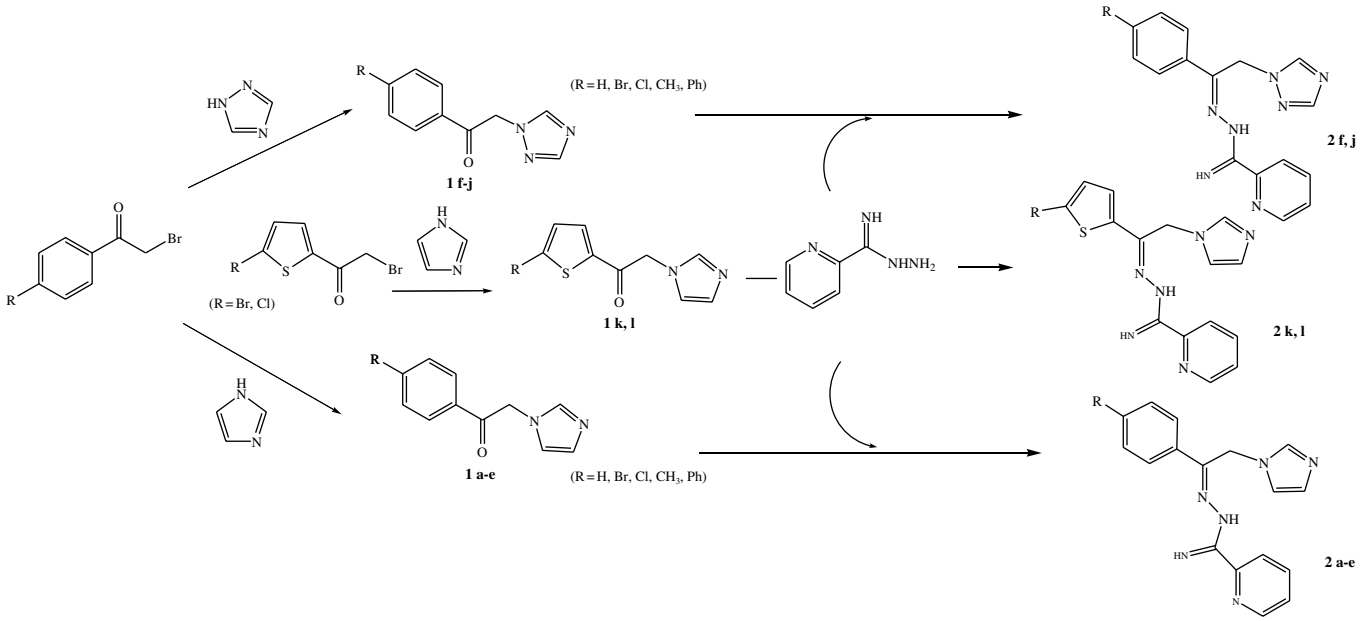

Figure 2. Synthesis of 12 new N^1-(1-aryl-2-(1*H*-imidazol-1-yl and 1*H*-1,2,4-triazol-1-yl)-ethylidene)-pyridine-2-carboxamidrazone derivatives, **2 a–l**.

Table 1. Effect of compounds **2 a–l** against 33 clinical isolates of *Candida spp.* (MIC_{90} = Minimum Inhibitory Concentration for 90% of strains)

	48 h MIC_{90} (mg/L)	
Compounds	*Candida albicans* (21)	*Candida glabrata* (12)
2 a–e	0.5–4	1–16
2 f–j	64	64
2 k–l	8	16
Amphotericin B	1	4
Miconazole	8	32

Table 2. Effect of compounds **2 a–l** against reference and clinical strains of *Mycobacterium tuberculosis*

	MIC (mg/L)	
Compounds	*M. tuberculosis* H37 Rv	*M. tuberculosis* H19, H21
2 a–e	8–32	4–32
2 f–j	32–64	32–64
2 k–l	8	4–16
Rifampicin	0.5	1
Miconazole	2	2

synthesized azole compounds interact with the target enzyme cytochrome P450-dependent sterol 14-α demethylase in the ergosterol biosynthesis pathway, through computer modelling of drug–enzyme complexes.[9] As stated above, the most active compounds were the halogenated bromo-phenyl and chloro-phenyl imidazolyl derivatives, for which MD simulations have been shown to yield free energy of binding values in harmony with the experimental microbiological findings.[9]

Table 2 lists the MICs of the newly synthesized compounds obtained by MRA[7] against different *M. tuberculosis* strains. All 12 azole compounds showed an interesting antitubercular killing activity, as demonstrated by viable count from MIC wells. Compounds **2a–e** had MICs in the range 4–32 mg/L against *M. tuberculosis* H37Rv reference strain and against two *M. tuberculosis* clinical strains, the methyl-phenyl and the phenyl imidazolyl derivatives **2b, 2c** and **2e** being the most active with an MIC of 4 mg/L for clinical isolates. The triazole derivative compounds **2f–j** had MICs in the range of 32–64 mg/L, while compounds **2k** and **l** (i.e. bromo-thienyl and chloro-thienyl imidazole derivatives) had promising antitubercular activity, with MICs in a range of 4–16 mg/L. Interestingly, the contribution to the killing activity, attributed to the different chemical moieties against *Mycobacterium*, appears not to be additive, since the azole antifungal drug miconazole and different 2-pyridinecarboxamidrazone derivatives[1,2] have been shown to possess a higher killing activity, characterized by lower MICs.

We also performed a preliminary study in order to predict how the newly synthesized azole compounds might interact with the target enzyme cytochrome P450-dependent 14DM of *M. tuberculosis* and *C. albicans* through computer modelling of the relevant drug–enzyme complexes. According to the procedure adopted, all 12 azole compounds were characterized by a similar docking mode in the active site of the 14DM from *M. tuberculosis*. The imidazole ring (compounds **2a–e** and **2k–l**) or triazole ring (compounds **2f–j**) is positioned almost perpendicular to the porphyrin plane, with a ring nitrogen atom coordinated to the haem iron. The analysis of the MD trajectories revealed that the average distance between N3(4) of the azole ring and the haem iron is 2.01 ± 0.4 Å, in good agreement with that found in the crystal structure of P450cam complexed with azole inhibitors.[52] The phenyl group of

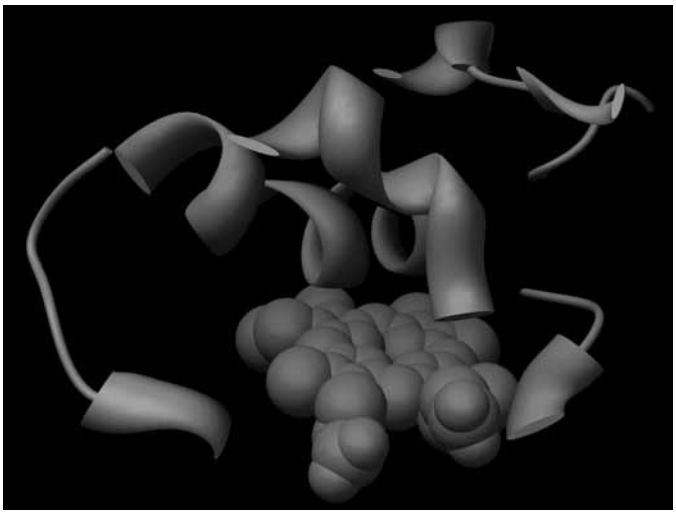

Figure 3. Cartoon of the secondary structural motifs of *Mycobacterium tuberculosis* sterol 14α- demethylase forming the protein active site. Light blue: β1-5-B′ helix (residues 76–84); light green: meander 1 (residues 87–94); light pink: helix F, C-terminus (residues 172–179); light grey: helix I (residues 249–261); light yellow: β6-1 sheet (residues 321–326); light brown: β6-2 sheet (residues 431–435). The haeme group is also shown in gold CPK representation.

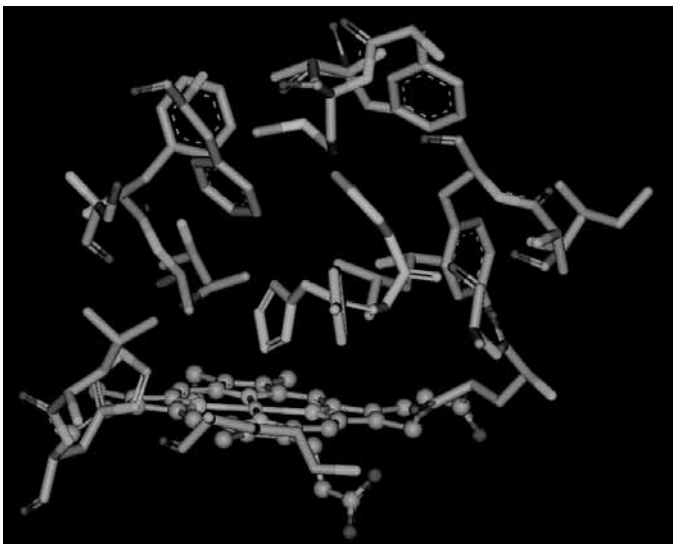

Figure 4. Equilibrated molecular dynamics snapshot of the docked compound **2c** in the active site of the sterol 14α-demethylase of *M. tuberculosis*. The haeme group is shown in atom-coloured ball-and-stick, the amino acids in atom-coloured stick and the compound **2c** in pink-coloured stick representation. For the sake of simplicity, only the amino acids pertaining to the active site or contacting compound **2c** are shown. Water molecules and hydrogen atoms are also omitted for clarity.

compounds **2a–j**, as well as the thienyl moiety of **2k–l**, locates in a hydrophobic binding cleft, above the haem ring. The active site residues interacting with the inhibitors consist of helix I, Meander 1, β6-1 (which composes the side of the active site), and β6-2, the C-terminus of helix F, and the β1-5-N-terminus of helix B′, which constitutes the dome of the active site (Figure 3). In particular, all hydrophobic substituents find location in a

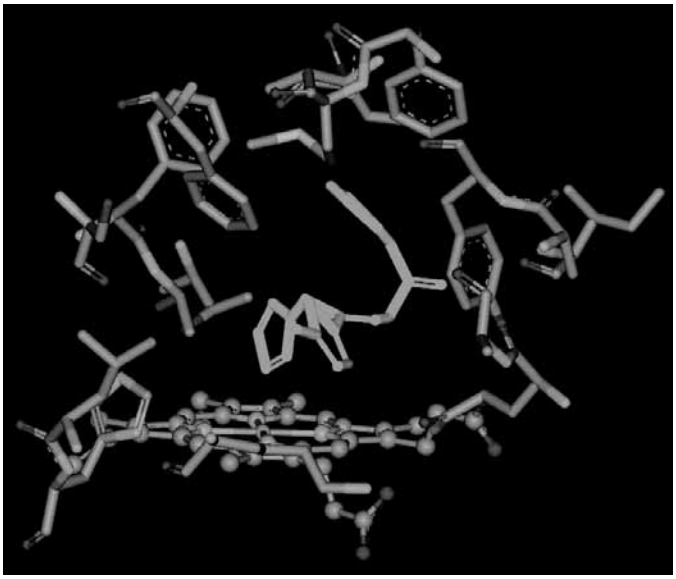

Figure 5. Equilibrated molecular dynamics snapshot of the docked compound **2l** in the active site of the sterol 14α-demethylase of *M. tuberculosis*. The haeme group is shown in atom-coloured ball-and-stick, the amino acids in atom-coloured stick and the compound **2l** in green-coloured stick representation. For the sake of simplicity, only the amino acids pertaining to the active site or contacting compound **2l** are shown. Water molecules and hydrogen atoms are also omitted for clarity.

hydrophobic subsite above the haem ring. The residue lining the subsite include the side chains of Q72, A73, A75, Y76, M79, F83, M99, L100, A256, L321, V434 and V435. Figures 4 and 5 show two equilibrated MD snapshots of the productive binding mode corresponding to compounds **2c** and **2l**, respectively.

The preferred, predicted orientation of all inhibitor series in the active site of *C. albicans* sterol 14DM is similar to that observed for *M. tuberculosis*, featuring the imidazole/triazole ring pointing orthogonally towards the haem plan and a ring nitrogen atom coordinating the iron ion. In this case, the main residues involved in the cleft encasing the phenyl group of compounds **2a–j**, and the thienyl moiety of **2k–l**, are F186, P187, H261, V460 and V461. The larger size of the phenyl ring extends the number of contacts in the binding site in comparison with those established by compounds characterized by the presence of the smaller thienyl ring. The pyridine ring, common to all inhibitors, is stabilized by favourable dispersion forces with the side chains of K98, L354, V355, P357 and Y359. Further stabilizing non-bonded interactions are established between the azole ring of the inhibitors and residues G254, M257, G258 and T262. Figures 6 and 7 report, as an example, two MD equilibrated snapshots of the *C. albicans* 14DM binding site in complex with compounds **2c** and **2l**.

More importantly in the framework of computer-assisted drug design, all calculated values for the total free energy of binding ΔG_{bind}, listed in Tables 3 and 4 for *M. tuberculosis* and *C. albicans*, respectively, are in harmony with the experimentally measured values of the corresponding MIC (see Tables 1 and 2 for comparison). In fact, there is an excellent agreement in the trend of ΔG_{bind} versus MIC within each enzyme–drug complex series.

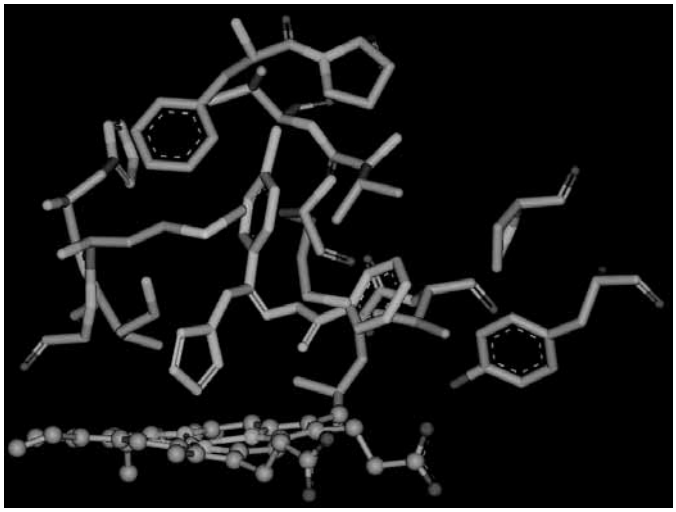

Figure 6. Equilibrated molecular dynamics snapshot of the docked compound **2c** in the active site of the sterol 14α-demethylase of *C. albicans*. The haeme group is shown in atom-coloured ball-and-stick, the amino acids in atom-coloured stick and the compound **2c** in green-coloured stick representation. For the sake of simplicity, only the amino acids pertaining to the active site or contacting compound **2c** are shown. Water molecules and hydrogen atoms are also omitted for clarity.

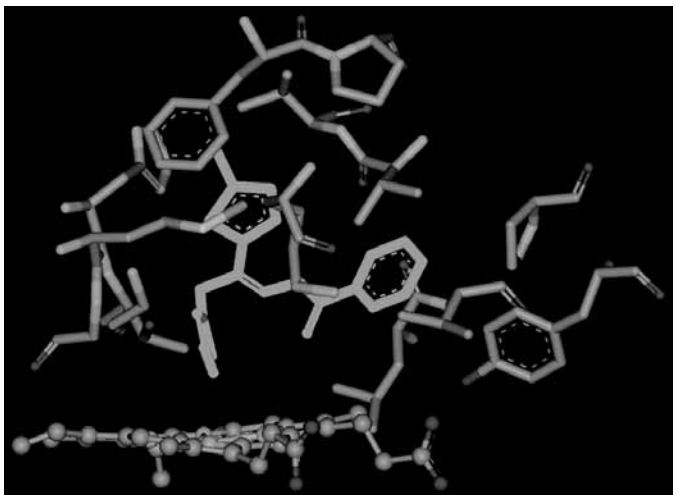

Figure 7. Equilibrated molecular dynamics snapshot of the docked compound **2l** in the active site of the sterol 14α-demethylase of *C. albicans*. The haeme group is shown in atom-coloured ball-and-stick, the amino acids in atom-coloured stick and the compound **2l** in green-coloured stick representation. For the sake of simplicity, only the amino acids pertaining to the active site or contacting compound **2l** are shown. Water molecules and hydrogen atoms are also omitted for clarity.

Further insights into the forces involved in substrate binding can be obtained by analysing the free energy components, which are listed in Tables 3 and 4 for all compounds in complex with *M. tuberculosis* and *C. albicans* 14DM, respectively. As seen in these Tables, both the intermolecular van der Waals and the electrostatics are important contributions to the binding. Comparing the van der Waals/non-polar ($\Delta E_{vdW} + \Delta G_{NP}$) with the electrostatic ($\Delta E_{EL} + \Delta G_{PB}$) contributions for all molecules, however, we see that in all cases the association between inhibitors and the target proteins is mainly driven by more favourable non-polar interactions in the complex than in solution. The total non-electrostatic components ($\Delta E_{vdW} + \Delta G_{NP}$) of the free energy of binding ΔG_{bind} are very similar for the series of compounds docked in both enzyme active sites (ranging from approximately –42 to –52 kcal/mol in the case of *M. tuberculosis*, and from –44 to –53 kcal/mol in the case of *C. albicans*). When examining the role of the electrostatics in the inhibitor–enzyme complex formation, however, it is fundamental to consider the electrostatic component of the molecular mechanical energy ΔE_{EL} together with the electrostatic contribution to solvation ΔG_{PB}. Indeed, electrostatics generally disfavour the docking of ligand and receptor molecules because the unfavourable change in the electrostatics of solvation is mostly, but not fully, compensated by the favourable electrostatics within thew resulting ligand–receptor complex. Indeed, the total electrostatic energy contributions for all 14DM–drug complex formations are unfavourable, the **2b–e/** and the **2k–l/**protein complex formations being less unfavourable than the remaining compound complex formations in both cases (see Tables 3 and 4) because of a less-positive total electrostatic term ($\Delta E_{EL} + \Delta G_{PB}$), in which the penalty paid by the electrostatics of solvation is better compensated by favourable electrostatic interactions within the complex. Thus, even though electrostatics destabilizes inhibitor–protein complex formation, it is the optimized balance of opposing electrostatic contributions that leads to tighter binding in the series of compounds **2b-e** and **2k–l** in the 14DM active site from both microorganisms.

Discussion

In the present work we report our recent efforts in design, synthesis and *in vitro* testing of a series of 12 new N^1-[1-aryl-2-(1*H*-imidazol-1-yl and 1*H*-1,2,4-triazol-1-yl)-ethylidene]-pyridine-2-carboxamidrazone derivatives as inhibitors of *M. tuberculosis* and *Candida* spp. Further, from the standpoint of a future integrated approach based on computer-assisted drug design, we contemporarily characterized their interaction with the active sites of sterol 14DM from both microorganisms.

Colour-based MRA gave good reproducible results employing inoculum suspensions of tubercular strains prepared directly from Lowenstein–Jensen slants, and good reproducible results were always obtained for MIC determinations of all new compounds. *In vitro* testing revealed that all new compounds had an interesting inhibiting activity against both microorganisms, the most active compounds being the halogenated (Br and Cl) derivatives **2b**, **2c**, **2k** and **2l**.

The application of combined docking-MM/PBSA free energy of binding calculations allowed us to rationalize the interactions between the entire series of 12 new inhibitors and the active sites of the 14DM enzyme from *M. tuberculosis* and *C. albicans*, both from a qualitative and most importantly from a quantitative point of view. Particularly, in the last case we verified an agreement between the trend in the calculated ΔG_{bind} values of all compounds and the corresponding experimental evidence, expressed in terms of MIC. Undoubtedly, further experimental evidence such a biological assay should be performed to confirm modelling prediction and the correctness of the chosen target.

Accordingly, the experimental data together with the computational evidence can be of use in further experimental

Table 3. Energy terms and total free energy of binding (kcal/mol) between sterol 14α-demethylase of *M. tuberculosis* and compounds **2a–l**

	2a	**2b**	**2c**	**2d**	**2e**	**2f**	**2g**	**2h**	**2i**	**2j**	**2k**	**2l**
ΔE_{vdW}	–37.22	–45.29	–47.90	–45.88	–44.77	–44.47	–40.27	–39.76	–40.44	–41.29	–44.66	–44.82
ΔE_{EL}	–15.51	–12.67	–12.55	–11.21	–15.54	–13.22	–13.63	–12.33	–12.61	–11.25	–14.83	–13.74
ΔE_{MM}	–52.73	–57.96	–60.45	–57.09	–60.31	–57.69	–53.90	–52.09	–53.05	–52.54	–59.49	–58.56
ΔG_{NP}	–4.38	–5.05	–4.10	–4.46	–4.99	–4.55	–4.08	–4.31	–4.32	–4.17	–4.21	–4.09
ΔG_{PB}	43.34	46.78	47.29	44.91	46.07	46.12	43.65	42.13	43.20	42.01	42.50	42.88
–TΔS	10.27	10.22	11.11	10.88	12.76	12.66	12.01	11.86	11.88	12.55	15.05	13.79
ΔG_{bind}	**–3.5**	**–6.01**	**–6.15**	**–5.76**	**–6.47**	**–3.46**	**–2.32**	**–2.41**	**–2.29**	**–2.15**	**–6.15**	**–5.98**

Table 4. Energy terms and total free energy of binding (kcal/mol) between sterol 14α-demethylase of *C. albicans* and compounds **2a–l**

	2a	**2b**	**2c**	**2d**	**2e**	**2f**	**2g**	**2h**	**2i**	**2j**	**2k**	**2l**
ΔE_{vdW}	–41.31	–48.30	–49.21	–42.91	–47.85	–43.28	–41.82	–39.66	–40.87	–41.25	–44.69	–43.28
ΔE_{EL}	–13.83	–14.66	–14.86	–15.84	–15.62	–13.11	–13.99	–15.64	–12.78	–11.25	–17.73	–16.74
ΔE_{MM}	–55.14	–62.96	–64.07	–58.75	–63.47	–56.39	–55.81	–55.30	–53.65	–52.50	–62.42	–60.02
ΔG_{NP}	–4.59	–5.10	–4.13	–4.21	–5.01	–4.43	–4.44	–4.66	–4.23	–4.20	–4.88	–4.55
ΔG_{PB}	44.33	46.78	45.19	44.22	46.01	45.86	44.15	43.89	44.01	43.16	44.66	43.88
–TΔS	10.27	10.65	11.89	11.21	12.72	12.69	12.01	11.56	11.88	11.32	14.85	12.79
ΔG_{bind}	**–5.13**	**–10.63**	**–11.12**	**–7.53**	**–9.75**	**–2.27**	**–4.09**	**–4.51**	**–1.99**	**–2.22**	**–7.79**	**–7.90**

protein–ligand design, since MD simulations have shown to be able to rank binding affinities of all inhibitors, and to provide insight into the interactions occurring in the active site and the origins of variations in the corresponding binding free energy, thus yielding invaluable information for the design and prediction of activity of a second generation of inhibitors within a reasonable length of computer and human time.

Acknowledgements

This work was supported by a financial funding of the Italian MIUR. S. P., M. F. and M. F. acknowledge the generous financial support of the Italian Ministry of University and Research (MIUR, Rome, Italy) in the framework of the FIRB 2001 project RBNE01J3SK_006. A preliminary account of this work was presented at 'World Conference on Magic Bullets to Celebrate Paul Ehrlich's 150th Birthday', 9–11 September 2004, Nurnberg, Germany.

Transparency declarations

None to declare.

References

1. Banfi E, Mamolo MG, Predominato M *et al. In vitro* antimycobacterial activity of new synthetic amidrazone derivatives. *J Chemother* 1993; **5**: 164–7.

2. Banfi E, Mamolo MG, Zampieri D *et al.* Antimycobacterial activity of N^1-(1-(3-aryl-1-(pyridin-2-, 3- or 4-yl)-3-oxo) propyl)-2-pyridinecarboxamidrazones. *J Antimicrob Chemother* 2001; **48**: 705–7.

3. Jackson CJ, Lamb DC, Kelly DE *et al.* Bactericidal and inhibitory effects of azole antifungal compounds on *Mycobacterium smegmatis*. *FEMS Microbiol Lett* 2000; **192**: 159–62.

4. Guardiola-Diaz HM, Foster LA, Mushrush D *et al.* Azole-antifungal binding to a novel cytochrome P450 from *Mycobacterium tuberculosis*: implications for the treatment of tuberculosis. *Biochem Pharmacol* 2001; **61**: 1463–70.

5. Zhang WJ, Ramamoorthy Y, Kilicarslan T *et al.* Inhibition of cytochromes P450 by antifungal imidazole derivatives. *Drug Metab Dispos* 2002; **30**: 314–18.

6. Bellamine A, Mangla AT, Ness WD *et al.* Characterization and catalytic properties of the sterol 14α-demethylase from *Mycobacterium tuberculosis*. *Proc Natl Acad Sci USA* 1999; **96**: 8937–42.

7. Banfi E, Scialino G, Monti-Bragadin C. Development of a microdilution method to evaluate *Mycobacterium tuberculosis* drug susceptibility. *J Antimicrob Chemother* 2003; **52**: 796–800.

8. Holtje HD, Folkers G. Molecular Modeling. Basic Principles and Applications. In: Mannhold R, Kubinyi H, Timmerman H, eds. *Methods and Principles in Medicinal Chemistry*. 1997 (5).

9. Mamolo MG, Zampieri D, Falagiani V *et al.* Antifungal and antimycobacterial activity of new N^1-(1-aryl-2-(1*H*-imidazol-1-yl and 1*H*-1,2, 4triazol-1-yl)ethylidene)-pyridine-2-carboxamidrazone derivatives: a combined experimental and computational approach. *Arkivoc* 2004; **5**: 231–50.

10. National Committee for Clinical Laboratory Standards. *Reference Method for Broth Dilution Antifungal Susceptibility Testing of Yeast. Approved standard M-27*. NCCLS, Villanova, PA, USA, 1997.

11. Podust LM, Poulos TL, Waterman MR. Crystal structure of cytochrome P450 14alpha-sterol demethylase (CYP51) from *Mycobacterium tuberculosis* in complex with azole inhibitors. *Proc Natl Acad Sci USA* 2001; **13**: 3068–73.

12. Case DA, Pearlman DA, Caldwell JW *et al.* AMBER 7, University of California, San Francisco, CA, USA, 2000.

13. Cornell W, Cieplak P, Bayly CI *et al*. A second generation force field for the simulation of proteins and nucleic acids. *J Am Chem Soc* 1995; **117**: 5179–97.

14. Paulsen MD, Ornstein RL. A 175-psec molecular dynamics simulation of camphor-bound cytochrome P-450cam. *Proteins* 1991; **11**: 184–204.

15. Jayaram B, Sprous D, Beveridge DL. Solvation free energy of biomacromolecules: parameters for a modified generalized Born model consistent with the AMBER force field. *J Phys Chem* 1998; **102**: 9571–6.

16. Marti-Renom MA, Stuart A, Fiser A *et al*. Comparative protein structure modeling of genes and genomes. *Annu Rev Biophys Biomol Struct* 2000; **29**: 291–325.

17. Sali A, Blundell TL. Comparative protein modeling by satisfaction of spatial restraints. *J Mol Biol* 1993; **234**: 779–815.

18. Sali A, Potterton L, Yuan F *et al*. Evaluation of comparative protein modeling by MODELLER. *Proteins* 1995; **23**: 318–26.

19. Boscott PA, Grant GH. Modeling cytochrome P450 14-α demethylase (*Candida albicans*) from P450cam. *J Mol Graph* 1994; **12**: 185–92.

20. Lamb DC, Kelly DE, Baldwin BC *et al*. Differential inhibition of *Candida albicans* CYP51 by stereoisomers of azole antifungals. *FEMS Microbiol Lett* 1997; **149**: 23–30.

21. Claessens M, VanCutsem E, Lasters I *et al*. Modeling the polypeptide backbone with 'spare parts' from known protein structures. *Protein Eng* 1989; **2**: 335–45.

22. Summers NL, Karplus M. Modeling of globular proteins. A distance-based data search procedure for the construction of insertion/deletion regions and Pro-non-Pro mutations. *J Mol Biol* 1990; **216**: 991–1016.

23. Levitt M. Accurate modeling of protein conformation by automatic segment matching. *J Mol Biol* 1992; **226**: 507–33.

24. Rossmann MG. Molecular replacement—historical background. *Acta Crystallogr D Biol Crystallogr* 2001; **57**: 1360–6.

25. Berendsen HJC, Postma JPM, van Gunsteren W *et al*. Molecular dynamics with coupling to an external bath. *J Chem Phys* 1984; **81**: 3684–90.

26. Andersen HC. Molecular dynamics simulations at constant pressure and/or temperature. *J Chem Phys* 1980; **72**: 2384–93.

27. Verlet L. Computer 'experiments' on classical fluids. I. Thermodynamical properties of Lennard-Jones molecules. *Phys Rev* 1967; **159**: 98–103.

28. Ryckaert JP, Ciccotti G, Berendsen HJC. Numerical-integration of cartesian equations of motion of a system with constraints - molecular-dynamics of N-alkanes. *J Comput Phys* 1977; **23**: 327–41.

29. Laskowski RA, MacArthur MW, Moss DS *et al*. PROCHECK: a program to check the stereochemical quality of protein structures. *J Appl Crys* 1993; **26**: 283–91.

30. Rhodriguez R, Chinea G, Lopez N *et al*. Homology modeling, model and software evaluation: three related resources. *CABIOS* 1998; **14**: 523–8.

31. Fermeglia M, Ferrone M, Pricl S. Computer-aided simulation of a dendrimer with a protoporphyrinic core as potential, novel hemoprotein mimic. *Bioorg Med Chem* 2002; **10**: 2471–8.

32. Felluga F, Pitacco G, Valentin E *et al*. Studying enzyme enantioselectivity using combined *ab initio* and free energy calculations: α-chymotrypsin and methyl cis- and trans-5-oxo-2-pentylpirrolidine-3-carboxylates. *Tetrahedron Asymmetry* 2003; **14**: 3385–99.

33. Manfredini S, Solaroli N, Angusti A *et al*. Design and synthesis of phosphonoacetic acid (PPA) ester and amide bioisosters of ribofuranosylnucleoside diphosphates as potential ribonucleotide reductase inhibitors and evaluation of their enzyme inhibitory, cytostatic and antiviral activity. *Antivir Chem Chemother* 2003; **14**: 183–94.

34. Mamolo MG, Zampieri D, Vio L *et al*. Antimycobacterial activity of new 3-substituted 5-(pyridin-4-yl)-3H-1,3,4-oxadiazol-2-one and 2-thione derivatives. Preliminary molecular modeling investigations. *Bioorg Med Chem* 2005; **13**: 3797–809.

35. Bayly CI, Cieplak P, Cornell WD *et al*. A well-behaved electrostatic potential based method using charge restraints for deriving atomic charges: the RESP model. *J Phys Chem* 1993; **97**: 10269–80.

36. Besler BH, Merz KM Jr, Kollman PA. Atomic charges derived from semiempirical methods. *J Comput Chem* 1990; **11**: 431–9.

37. Singh UC, Kollman PA. An approach to computing electrostatic charges for molecules. *J Comput Chem* 1984; **5**: 129–45.

38. Morris GM, Goodsell DS, Halliday RS *et al*. Automated docking using a lamarckian genetic algorithm and an empirical binding free energy function. *J Comput Chem* 1998; **19**: 1639–62.

39. Mehler EL, Solmajer T. Electrostatic effects in proteins: comparison of dielectric and charge models. *Protein Eng* 1991; **4**: 903–10.

40. Frecer V, Kabelac M, De Nardi P *et al*. Structure-based design of inhibitors of NS3 serine protease of hepatitis C virus. *J Mol Graph Model* 2004; **22**: 209–20.

41. Metullio L, Ferrone M, Coslanich A *et al*. Polyamidoamine (yet not PAMAM) dendrimers as bioinspired materials for drug delivery: structure-activity relationships by molecular simulations. *Biomacromolecules* 2004; **5**: 1371–8.

42. Fermeglia M, Ferrone M, Lodi A *et al*. Host-guest inclusion complexes between anticancer drugs and beta-cyclodextrin: computational studies. *Carbohydr Polym* 2003; **53**: 15–44.

43. Jorgensen WL, Chandrasekhar J, Madura JD *et al*. Comparison of simple potential functions for simulating liquid water. *J Chem Phys* 1983; **79**: 926–35.

44. Darden T, York D, Pedersen L. Particle mesh Ewald—an N.log(N) method for Ewald sums in large systems. *J Chem Phys* 1993; **98**: 10089–92.

45. Srinivasan J, Cheatham TE, Cieplak P *et al*. Continuum solvent studies of the stability of DNA, RNA, and phosphoramidate—DNA helices. *J Am Chem Soc* 1998; **120**: 9401–9.

46. Gilson MK, Sharp KA, Honig B. Calculating the electrostatic potential of molecules in solution: method and error assessment. *J Comput Chem* 1987; **9**: 327–35.

47. Chong LT, Duan Y, Wang L *et al*. Molecular dynamics simulation and free energy calculations applied to affinity maturation in antibody 48G7. *Proc Natl Acad Sci USA* 1990; **96**: 14330–5.

48. Sitkoff D, Sharp KA, Honig B. Accurate calculation of hydration free energies using macroscopic solvent models. *J Phys Chem* 1994; **98**: 1978–88.

49. Sanner MF, Olson AJ, Spehner JC. Reduced surface: an efficient way to compute molecular surfaces. *Biopolymers* 1996; **38**: 305–20.

50. Wilson EB, Decius JC, Cross PC. *Molecular Vibrations*. New York, NY: McGraw-Hill, 1995.

51. Pricl S, Fermeglia M, Ferrone M *et al*. T315I-mutated Bcr-Abl in chronic myeloid leukemia and imatinib: insights from a computational study. *Mol Cancer Ther* 2005; **4**: 1167–74.

52. Raag R, Li H, Jones BC *et al*. Inhibitor-induced conformational change in cytochrome P-450CAM. *Biochemistry* 1993; **32**: 4571–8.